Shi, Junjie; Han, Nana; Jin, Benjin; Suominen, Milla; Lahtinen, Jouko; Miikki, Kim; Wilson, Benjamin P.; Kallio, Tanja

Construction of hydrophilic-hydrophobic domains in Bi_2O_3/nitrogen-doped carbon electrode to boost CO_2-to-formate conversion

Published in:
Next Materials

DOI:
10.1016/j.nxmate.2024.100183
10.1016/j.nxmate.2024.100183

Published: 01/04/2024

Document Version
Publisher's PDF, also known as Version of record

Please cite the original version:
Shi, J., Han, N., Jin, B., Suominen, M., Lahtinen, J., Miikki, K., Wilson, B. P., & Kallio, T. (2024). Construction of hydrophilic-hydrophobic domains in Bi_2O_3/nitrogen-doped carbon electrode to boost CO_2-to-formate conversion. *Next Materials*, *3*, Article 100183. https://doi.org/10.1016/j.nxmate.2024.100183, https://doi.org/10.1016/j.nxmate.2024.100183

Next Materials 3 (2024) 100183

Contents lists available at ScienceDirect

Next Materials

journal homepage: www.sciencedirect.com/journal/next-materials

Research article

Construction of hydrophilic-hydrophobic domains in Bi_2O_3/nitrogen-doped carbon electrode to boost CO_2-to-formate conversion

Junjie Shi [a], Nana Han [a], Benjin Jin [a], Milla Suominen [a], Jouko Lahtinen [b], Kim Miikki [c], Benjamin P. Wilson [d], Tanja Kallio [a,*]

[a] Department of Chemistry and Materials Science, School of Chemical Engineering, Aalto University, P.O. Box 16100, Aalto 00076, Finland
[b] Department of Applied Physics, School of Science, Aalto University, P.O. Box 15100, Aalto 00076, Finland
[c] School of Chemical Engineering, Aalto University, P.O. Box 16100, Aalto 00076, Finland
[d] Department of Chemical and Metallurgical Engineering, School of Chemical Engineering, Aalto University, P.O. Box 16200, Aalto 00076, Finland

ARTICLE INFO

Keywords:
CO_2 electrochemical reduction
Nitrogen-doped carbon support
Surface hydrophobicity
Hydrophilic-hydrophobic domains
Triple-phase interfaces

ABSTRACT

Bi has drawn attention in catalyzing the electrochemical CO_2-to-formate conversion due to promising selectivity and low cost, but the process suffers from low activity. Herein, we introduce nitrogen-doped carbon (NC) support with hydrophobicity modification to enhance the activity of a binder-free Bi_2O_3 electrode. Formate partial current on the NC supported Bi_2O_3 electrode almost doubles compared to Bi_2O_3 on unmodified support. Furthermore, the hydrophobicity modification with polytetrafluoroethylene (PTFE) significantly extends the stability of NC supported Bi_2O_3 by diminishing flooding. It also maintains >90% formate selectivity at a broad potential range from -0.87 to -1.27 V (vs. RHE) and shows a formate partial current density of -100 mA cm^{-2} at -1.37 V (vs. RHE) in 0.5 M $KHCO_3$. The improvement is attributed to the synergetic effects of the hydrophilic active sites and the hydrophobic PTFE modified NC support. The unique structure promotes the reactants transport and thus maximizes the active site utilization at the triple-phase interface. This facile microenvironment regulation can be extended to other applications involving gaseous-aqueous phases.

1. Introduction

CO_2 electrochemical reduction reaction (CO_2RR) presents a viable method for closing the carbon loop by employing renewable energy sources to transform CO_2 into useful chemicals or fuels [1,2]. The production of formate is a practical procedure that requires only two-electron transfer, and the reaction takes place at a reasonably good selectivity. In addition, formic acid/formate has the best economic value when the cost of energy input is considered [3].

Bi catalysts have attracted considerable interest in electrochemical CO_2-to-formate conversion owing to excellent selectivity with low environmental impact, abundant availability, and affordable price [4,5]. High selectivity is attributed to ideal binding of CO_2 reduction intermediates and hydrogen on Bi which promotes CO_2-to-formate formation while effectively suppressing the competing hydrogen evolution reaction [3,5]. However, Bi-electrocatalysts still suffer from low efficiency in near neutral electrolytes as high selectivity and catalytic current density cannot be attained at low overpotentials [6–10]. Although high catalytic activities can be achieved in alkaline electrolytes [11,12], the process remains problematic as CO_2 is mainly consumed in the alkaline electrolyte through a reaction with the hydroxide ions to produce carbonates. This creates issues in the downstream liquid product separation process [13]. In this scenario, CO_2RR on Bi-based electrodes in near-neutral electrolytes can offer a viable approach if the performance of the catalyst is improved.

Various modifications have been studied to improve the performance of Bi-electrocatalysts such as morphology tuning [14,15], doping [16,17], alloying [18,19], and supporting [20–25]. Among these strategies, depositing Bi nanostructures on various supports is one of the most efficient strategies, as it can avoid agglomeration and confine the size of the active materials. Nitrogen-doped carbon (NC) is widely used as a support for Bi-electrocatalysts since both charge transfer and $CO_2/CO_2^{\bullet-}$ adsorption can be promoted with the introduction of NC [21–25].

When the catalyst is directly grown on a support, use of costly polymer binders (like Nafion) with a naturally insulating property is avoided. It improves the electron transport and active site accessibility [26–28] compared to alternative approach, which includes mixing of catalyst particles with a binder. Another benefit of the binder-free

---

* Corresponding author.
E-mail address: tanja.kallio@aalto.fi (T. Kallio).

https://doi.org/10.1016/j.nxmate.2024.100183
Received 20 November 2023; Received in revised form 2 February 2024; Accepted 19 March 2024

configuration is that it allows us to study the active materials without such secondary effects as the type [29], content [30], and dispersion solvent [31] of binder, which can influence the performance. However, only a few reported NC supported Bi_2O_3 electrodes were designed for efficient CO_2-to-formate conversion, combining the advantages of a NC support and binder-free electrode architecture [24]. Nevertheless, the narrow potential range of formate production still hinders its practical application, as in industrial production typically the production rate, i.e. current, is fixed while potential fluctuates. It is imperative to fabricate well-performing binder-free NC supported Bi-based electrodes for CO_2-to-formate conversion in a wide potential range, and further comprehensively study the active materials.

Binders also greatly affect the wettability of the electrodes, which is another important aspect in CO_2RR as it influences the adsorption and transport of reactants and products at a solid−liquid−gas triple-phase interface [32,33]. A super hydrophilic electrode surface might result in flooding and the loss of gas transport pores, which may be a reason for the narrow formate selective potential range of the above-mentioned NC supported Bi_2O_3 electrodes [24]. A very hydrophobic electrode, on the other hand, does not allow for enough contact between the electrode and electrolyte [33]. As a result, efforts have been made to adjust the electrode wettability by modulating the catalyst [34–41] or the support [11,42,43]. For instance, organic chemicals modified Cu-based materials [37,38,40] and polytetrafluoroethylene (PTFE)-modified NC nanotube [35] could generate hydrophobic surfaces which can trap CO_2 close to active sites and further enhance the performance, while Bi_2O_3 on hydrophobic carbon fiber outperforms Bi_2O_3 on hydrophilic ones [11]. However, even though notable attempts have been made, systemic comparisons between these two wettability approaches are still missing in existing studies. Besides, none of them emphasizes widely used NC supports.

To fabricate an efficient NC supported Bi-based electrodes, wettability modulation and systemic comparisons between different wettability approaches, particularly when employing a binder-free electrode structure, are required to be explored. To that end, we fabricated binder-free Bi_2O_3 on a carbon cloth (Bi_2O_3) and first improved its CO_2RR efficiency by introducing a NC support (Bi_2O_3@NC). This resulted in initial improvements in reducing the overpotential for formate production by more than 200 mV and nearly doubled the current density in 0.5 M $KHCO_3$. However, changes in the hydrophilicity of the support led to instability and undesirable enhancement of hydrogen evolution at high overpotentials. Therefore, we set investigating the effects of different hydrophobic modifications. Our results show that it is preferable to alter the surface hydrophobicity by modification of the support rather than the catalyst layer itself. Optimum CO_2-to-formate condition is achieved with the coexistence of hydrophilic Bi_2O_3 on a hydrophobic PTFE-modified NC support (Bi_2O_3@PTFE-NC). The unique structure mitigates the flooding issue effectively. Bi_2O_3@PTFE-NC electrode displays over 90% Faradaic efficiency (FE) to formate in a broad potential region from −0.87 V to −1.27 V (vs. RHE) with a maximum value of 94.9% at −0.97 V (vs. RHE). Our systematic approach for constructing hydrophilic-hydrophobic electrodes can be further applied to improve electrocatalytic reactions involving both gaseous/aqueous phases on the electrode surface.

2. Experimental details

2.1. Materials

Bismuth (III) nitrate pentahydrate ($Bi(NO_3)_3 \cdot 5\,H_2O$, 98.0%), Zinc nitrate hexahydrate ($Zn(NO_3)_2 \cdot 6\,H_2O$, 98.0%), 2-methylimidazole (2-MI, 99.0%), Polytetrafluoroethylene preparation (60 wt% dispersion in H_2O), Ethylene glycol (ReagentPlus®, ≥99.0%), Potassium permanganate ($KMnO_4$, ≥99.0%), Nafion dispersion (5 wt%), 2-Propanol (suitable for HPLC, 99.9%), and potassium bicarbonate ($KHCO_3$, 99.7%) were purchased from Sigma-Aldrich. Ethanol AA grade was purchased from Altia Oyj. All chemicals were used without further purification. Water from a Synergy purification system (18.2 MΩ cm at 25 °C) was used to prepare all aqueous solutions. Carbon Cloth (CC, ELAT-H) of a thickness of 406 μm was purchased from FuelCellsEtc and cut into 2.5 cm×2.5 cm pieces. Nafion 115 membrane was purchased from Ion Power and treated with 5% H_2O_2 for 60 min, water for 30 min, 0.5 M H_2SO_4 for 60 min, and finally, 3 times in water all at 100 °C. CO_2 (99.995%) from Woikoski was used as supplied. Leak-free Ag/AgCl reference electrode from Innovative Instruments was used as supplied.

2.2. Electrode preparation

Synthesis of Nitrogen-doped carbon nanosheet array (NC) anchored on CC: Zeolite imidazolate framework-8 (ZIF-8) is used as precursor for NC synthesis by a method adapted from a previous report with minor changes [44]. In short, CC was pretreated with 0.5 M $KMnO_4$ for 30 min, thoroughly washed, and dried. 40 mL of 0.05 M $Zn(NO_3)_2$ and 40 mL of 0.4 M 2-methylimidazole were stirred vigorously for 1 min, and after that, a piece of pretreated CC was placed vertically in the mixture and aged for 2 h to grow ZIF-8 coating on CC. Subsequently, the ZIF-8 coated CC was rinsed with ethanol 3 times before being dried at 80 °C in the oven for 1 h. NC was synthesized through pyrolysis of ZIF-8 coated CC in an N_2 atmosphere at 800 °C for 2 h with a heating rate of 1 $^{\circ}C\ min^{-1}$, followed by soaking in 0.5 M H_2SO_4 overnight to remove the zinc residue. After rinsing several times with water and ethanol, the NC-coated electrode was dried at 80 °C in the oven for 2 h.

Synthesis of PTFE-modified NC (PTFE-NC) anchored on CC: The as-prepared NC coated electrode was dipped 3 times in 0.2 wt% PTFE solution and dried at 80 °C in the oven for 2 h. The as-obtained supports were further heated in the N_2 atmosphere at 350 °C for 30 min with a heating rate of 5 $^{\circ}C\ min^{-1}$ to remove the surfactant in the PTFE solution. Other concentrations such as 0.1, 0.25, and 0.3 wt% PTFE solutions were also used in the optimization procedure.

Synthesis of PTFE-modified CC (PTFE-CC): CC was dipped 3 times in 0.2 wt% PTFE solution and dried at 80 °C in the oven for 2 h. The as-obtained supports were further heated in the N_2 atmosphere at 350 °C for 30 min with a heating rate of 5 $^{\circ}C\ min^{-1}$ to remove the surfactant in the PTFE solution.

Growth of Bi_2O_3 on the supports (Bi_2O_3, Bi_2O_3@PTFE-CC, Bi_2O_3@NC, and Bi_2O_3@PTFE-NC): BiO_{2-x} was grown on CC, PTFE-CC, NC, and PTFE-NC through a modified solvothermal method adapted from a previous report, respectively [26,45]. In a typical procedure, 1 mmol of $Bi(NO_3)_3 \cdot 5\,H_2O$ was dissolved in 6 mL of ethylene glycol by sonication followed by the addition of 12 mL of ethanol to form a homogeneous solution. A piece of the support was placed aslant in the autoclave and stood for 1 h before thermal treatment at 160 °C for 5 h. After the solvothermal reaction, the electrode was repeatedly rinsed with ethanol and dried at 80 °C in the oven for 2 h. The as-obtained samples were further calcinated in the air at 300 °C for 1 h with a heating rate of 5 $^{\circ}C\ min^{-1}$ to convert BiO_{2-x} into β-Bi_2O_3 [46].

Synthesis of PTFE-modified Bi_2O_3@NC: BiO_{2-x} (before calcination in the air) was dipped 3 times in diluted PTFE solution. The concentration of the PTFE solution was again varied between 0.1, 0.2, 0.25, and 0.3 wt%. The electrode was then dried at 80 °C in the oven for 2 h, and the as-obtained samples were further calcinated in air at 300 °C for 1 h with a heating rate of 5 $^{\circ}C\ min^{-1}$ to remove the surfactant in the PTFE solution [47] and convert BiO_{2-x} into β-Bi_2O_3 [46].

Air-brushed Bi_2O_3/Nafion: 16 mg Bi_2O_3 was dispersed in a mixture of 160 μL Nafion dispersion and 240 μL 2-propanol by sonication. The as-prepared ink was airbrushed on CC to acquire the loading with approximately 1.5 mg cm^{-2}.

2.3. Phys-chemical characterizations

X-ray diffraction (XRD): The crystal structure was characterized with XRD using a Rigaku diffractometer and Cu Kα radiation (λ =

0.15418 nm, 45 kV, 40 mA) in a 2θ range of 10° to 90° with a scan step size of 0.02°.

Raman: Raman spectra were recorded on Renishaw inVia™ QONTOR Raman spectrometer instrument equipped with a 532 nm laser and a CCD detector.

Transmission electron microscopy (TEM): Images of the samples were obtained using a JEOL JEM-2800FS microscope at an accelerating voltage of 200 kV.

Scanning electron microscopy (SEM): Images of the samples were obtained using a Tescan Mira3 microscope at an accelerating voltage of 15 kV and 5 kV for supports and Bi_2O_3 on supports, respectively. SEM-EDS images were taken using a JEOL JIB-4700 F at an accelerating voltage of 15 kV.

X-ray photoelectron spectroscopy (XPS): XPS measurements were made using the Kratos Axis Ultra system, equipped with a monochromatic Al-K_α X-ray source. All measurements were performed with a 0.3 mm×0.7 mm analysis area and the charge neutralizer. The wide scans were performed with 80 eV pass energy and 1 eV energy step, and the high-resolution scans were performed with 40 eV pass energy and 0.1 eV step size. The energy calibration was made using the adventitious carbon C 1 s component at 284.8 eV. All decompositions were made with CasaXPS using GL (30) peaks (product of 30% Lorentzian and 70% Gaussian).

CO_2 adsorption: CO_2 gas adsorption experiments at −0.15 °C (273 K) were carried out using a MicrotracBEL BELSorp MAX II (Microtrac BEL) equipment with integrated cooling bath. Samples were pretreated under vacuum at 300°C for 5 hours using a Microtrac BEL-Prep Vac II Pre-Treatment Station (Microtrac MRB) prior to measurement.

Contact angle measurement: Contact angle measurements were made using Theta Flex optical tensiometer with 12 μL CO_2-saturated 0.5 M $KHCO_3$.

CO_2 bubble adhesion experiment: The electrode is placed horizontally with a clamp and immersed in CO_2 buffered 0.5 M $KHCO_3$. Images of CO_2 bubble adhesion on the electrode were taken by an open-source High-Speed Camera System [48], and the volume of a gas bubble is approximately 12 μL.

2.4. Electrochemical tests

Electrochemical flow cell for CO_2RR: CO_2 electroreduction reactions were performed at room temperature using CO_2 buffered 0.5 M $KHCO_3$ (pH=7.3) in a flow cell (see the configuration in Scheme S1 and in our recently reported article [49]) coupled with an IviumStat.XRi potentiostat. A Bi_2O_3 on the support (Bi_2O_3, Bi_2O_3@NC, Bi_2O_3@-PTFE-NC, and PTFE-modified Bi_2O_3) or a support (CC, NC, and PTFE-NC) was directly used as a working electrode (area 2 cm ×2 cm), an Iridium Mixed Metal Oxide (MMO) plate was used as a counter electrode and a leak-free Ag/AgCl electrode was used as a reference electrode. CO_2 was directly bubbled onto the working electrode at 11 mL min^{-1}, and the electrolyte flow rate was controlled at 11 mL min^{-1}.

CO_2 was purged for at least 30 min before 10 cyclic voltammetry (CV) cycles were performed from −0.90 V to −1.90 V (vs. Ag/AgCl) at a scan rate of 50 mV s^{-1}. After recording the CVs, electrolysis was performed with a controlled-potential method from −1.30 V to −2.00 V (vs. Ag/AgCl). During the electrolysis, the gaseous products were monitored by micro gas chromatography (GC, Agilent 990) with two columns, MoleSieve 5 A and PoraPlot, and micro-machined TCD detectors. Liquid products were collected and quantified when electrolysis was finished using High-Performance Liquid Chromatography (HPLC) coupled to AMinex column HPX-87X from BioRad and RI detector.

Faradaic Efficiency (FE) of gaseous product i (CO or H_2) is calculated using the equation below:

$$FE(i) = \frac{Q_i}{Q_{total}} = \frac{I_i}{I} = \frac{ZF\varnothing_i v}{I}$$

Z: charge transfer per mole of gas product, in our case Z=2;
F: Faraday constant, 96485 C mol^{-1};
$\varnothing_i$: volume fraction of gaseous product quantified by GC;
v: molar flow rate of CO_2, mol s^{-1};
I: total current when GC sampling, A.

FE of formate is calculated using the equation below:

$$FE(formate) = \frac{Q_{formate}}{Q_{total}} = \frac{ZFc_{formate}V}{It}$$

c_{formate}: concentration of formate quantified by HPLC, mol L^{-1};
V: total volume of catholyte, L;
I: total current of electrolysis, A;
t: time of electrolysis, s.

Impedance was collected from 1000 Hz to 1 Hz. Applied potentials were automatically corrected by instruments with built-in 85% *iR* compensation and converted to the reversible hydrogen electrode (RHE) scale according to the equation shown below:

$$E(RHE) = E(Ag/AgCl) + 0.2 + 0.0591pH$$

Double-layer capacitance (C_{dl}): C_{dl} was determined by recording CVs of working electrodes between −0.1 V and −0.2 V (vs. Ag/AgCl, 3 M KCl) at different scan rates varying from 20 to 120 mV s^{-1} in CO_2 buffered 0.5 M $KHCO_3$. An iridium wire was used as a counter electrode.

3. Results and discussion

3.1. Synthesis and characterizations of electrodes

Different supports were first prepared and Bi_2O_3 was then anchored as explained in the **Methods** section and shown in Scheme 1. Firstly, NC was anchored on CC through pyrolysis of Zn-based zeolitic imidazolate framework (ZIF-8) [44]. The successful synthesis of NC was confirmed by SEM, TEM, Raman, and XRD (Figures S1 and S2). NC arrays maintain the nanosheet morphology of ZIF-8 after pyrolysis and acid wash (Figure S1b-c), which is consistent with the reported literature [44]. Only D-band at 1350 cm^{-1} and G-band at 1590 cm^{-1} are visible in the Raman spectrum of CC (Figure S2a), while additional A-bands between the D- and G-band resulting from assorted vibrations caused by the presence of heteroatoms become visible in NC (Figure S2b) [50] indicating a successful synthesis. The insertion of nitrogen and removal of Zn were further proved by EDS in Figure S1f-g (N content >8 at% while Zn almost completely removed, ≤0.03 at%). To increase the hydrophobicity of the NC support, PTFE was added to modify the surface (PTFE-NC). After the modification, the NC arrays were partially covered with melting polymer particles as shown in Fig. 1a. The Raman spectrum of PTFE-NC is similar to the one of NC, proving the surface defects did not change during the PTFE modification (Figure S2c).

Secondly, Bi_2O_3 was grown on three supports (CC, NC, and PTFE-NC) by a widely used solvothermal method and subsequent calcination in air. As shown in Fig. 1b and Figure S3a-c, Bi_2O_3 nanosheets are densely and uniformly grown on the supports. In this way, the active material can form intimate contact with the supports, which could boost charge transfer [26,51]. These nanosheets overlap and interconnect with each other to form large macropores. The secondary structure of an individual nanosheet was further examined by TEM in Fig. 1c-d revealing that each nanosheet is composed of connected nanoparticles of a size of around 10 nm with lattice fringes of 0.319 nm corresponding to the (201) lattice spacing of β-Bi_2O_3 [52,53]. The porous structure with both macropores and nanopores is advantageous for mass transfer and provides abundant

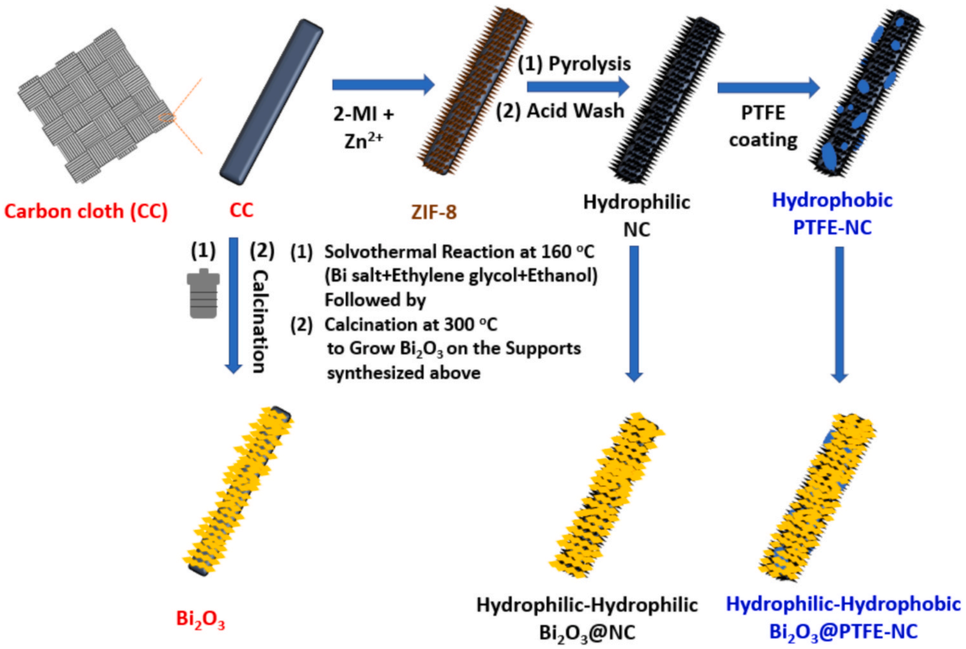

Scheme 1. Schematic illustration for the synthesis of Bi_2O_3, Bi_2O_3@NC, and Bi_2O_3@PTFE-NC.

active sites for CO_2RR. In contrast, Bi_2O_3 airbrushed on CC with the aid of the Nafion binder (air-brushed Bi_2O_3/Nafion) shows inhomogeneous distribution of large catalyst aggregates and Nafion covered surface (Figure S3d).

The crystal structure is fine β-Bi_2O_3 (PDF#27–0050) [46,54], which is confirmed by XRD shown in Fig. 1e. The peak at 26° is the (002) plane of graphitized carbon from the supports (Figure S2d). The chemical composition of the samples (Fig. 1f-h, and Figure S4) was characterized by using XPS. The peaks at 159.20 and 164.60 eV in the high-resolution Bi 4 f spectrum (Fig. 1f) of Bi_2O_3 correspond to Bi^{3+} in the Bi_2O_3 component. In the Bi_2O_3@NC sample, the Bi 4 f peaks shift to the slightly higher binding energy of 159.35 and 164.75 eV, which may result from the interaction between Bi_2O_3 and NC. A similar observation has been made when Bi_2O_3 was anchored on polydopamine-derived NC [24]. The Bi 4 f peaks in the Bi_2O_3@PTFE-NC sample show nearly the same positions as those in the Bi_2O_3@NC sample. Pyrrolic-N (at 400.5 eV) and pyridinic-N (at 398.4 eV) both dominate the N states with pyridinic-N composing more than 70 at% in both Bi_2O_3@NC and Bi_2O_3@PTFE-NC, which is shown in the high-resolution N 1 s XPS spectra (Fig. 1g). N species in NC have been reported to facilitate CO_2 capture [55] which is beneficial for electrocatalytic processes as more CO_2 can also be utilized by the neighboring Bi_2O_3. Both the pyrrolic-N and pyridinic-N in NC have been proven to effectively promote CO_2-to-formate in bismuth/NC electrocatalysts by a previous study [22]. The F 1 s signal present in Bi_2O_3@PTFE-NC originates from the PTFE particles coated on the NC support (Fig. 1h).

All the characterizations show that we successfully synthesized binder-free electrodes composed of both supports and Bi_2O_3. The morphology, crystal structure, and chemical composition of Bi_2O_3 show minor changes after the introduction of NC, which could be further used to rationally evaluate the influence of NC supports on the performance of CO_2RR.

3.2. *Performance comparison of Bi_2O_3 and Bi_2O_3@NC*

A customized flow cell was used to evaluate the catalytic performance of Bi_2O_3 and Bi_2O_3@NC directly as working electrodes in a CO_2-buffered 0.5 M $KHCO_3$ electrolyte. Bi_2O_3@NC exhibits slightly lower onset potential and higher current density in preliminary cyclic voltammetry (CV) measurements compared to Bi_2O_3 as shown in Figure S5. Electrolysis was further carried out on a subset of applied potentials ranging from −0.67 V to −1.37 V (vs. RHE) based on the CVs to define preferable conditions for CO_2RR. Through analysis of gaseous and liquid reduction products over Bi_2O_3 and Bi_2O_3@NC, only three products are found, which are H_2, a trace amount of CO, and mainly formate. The selectivity and current density are displayed in Fig. 2a-b, Figure S6a-e, and Table S1. FE of the target product formate on Bi_2O_3 increases with increasing overpotential in the range from −0.67 V to −1.17 V (vs. RHE) before gradually declining. On this electrode, the FE of formate achieves over 90.0% selectivity at −0.97 V (vs. RHE) and reaches the highest value of 95.6% at −1.17 V (vs. RHE). Formate production rate on an air-brushed Bi_2O_3/Nafion electrode is lower than on Bi_2O_3 (Figure S6f), which is in line with the reported literature [26]. Bi_2O_3@NC reaches ≥90% formate FE at lower overpotentials (−0.87 V vs. RHE) when compared to Bi_2O_3. The partial current density of formate production of both Bi_2O_3 and Bi_2O_3@NC increase as more negative potentials are applied, with Bi_2O_3@NC showing more than 2 times the formate partial current density compared to Bi_2O_3 at most potentials. Notably, Bi_2O_3@NC reaches $-23.8\ mA\ cm^{-2}$ at −0.97 V (vs. RHE) while more than 200 mV higher overpotential is required for Bi_2O_3, which achieves a comparable current density value at −1.17 V (vs. RHE).

The electrochemically active surface area (ECSA) was evaluated using the double-layer capacitance (C_{dl}) and the results are shown in Fig. 2c and Figure S7. C_{dl} of Bi_2O_3@NC is approximately 36% higher than C_{dl} of Bi_2O_3 (1.18 vs. 0.87 $mF\ cm^{-2}$, respectively). Modification of Bi_2O_3 with NC also enhances the volume of gas (CO_2) assimilated by the material, with an approximately 3 times measured increase in the level of CO_2 adsorbed by Bi_2O_3@NC when compared with unmodified Bi_2O_3 (Figure S8). This lowers the charge transfer resistance from 24.38 Ohms for Bi_2O_3 to 20.18 Ohms for Bi_2O_3@NC (Fig. 2d).

A well-accepted mechanism of the two-electron reduction of CO_2 to $HCOO^-$ on Bi-electrocatalysts follows the steps below [4,56,57] in [Eqs. (1), (2), (3), (4), and (5)]:

$$CO_2\ (solution) \rightarrow CO_2\ (ads) \tag{1}$$

$$CO_2(ads) + e^- \rightarrow CO_2^{*-} \tag{2}$$

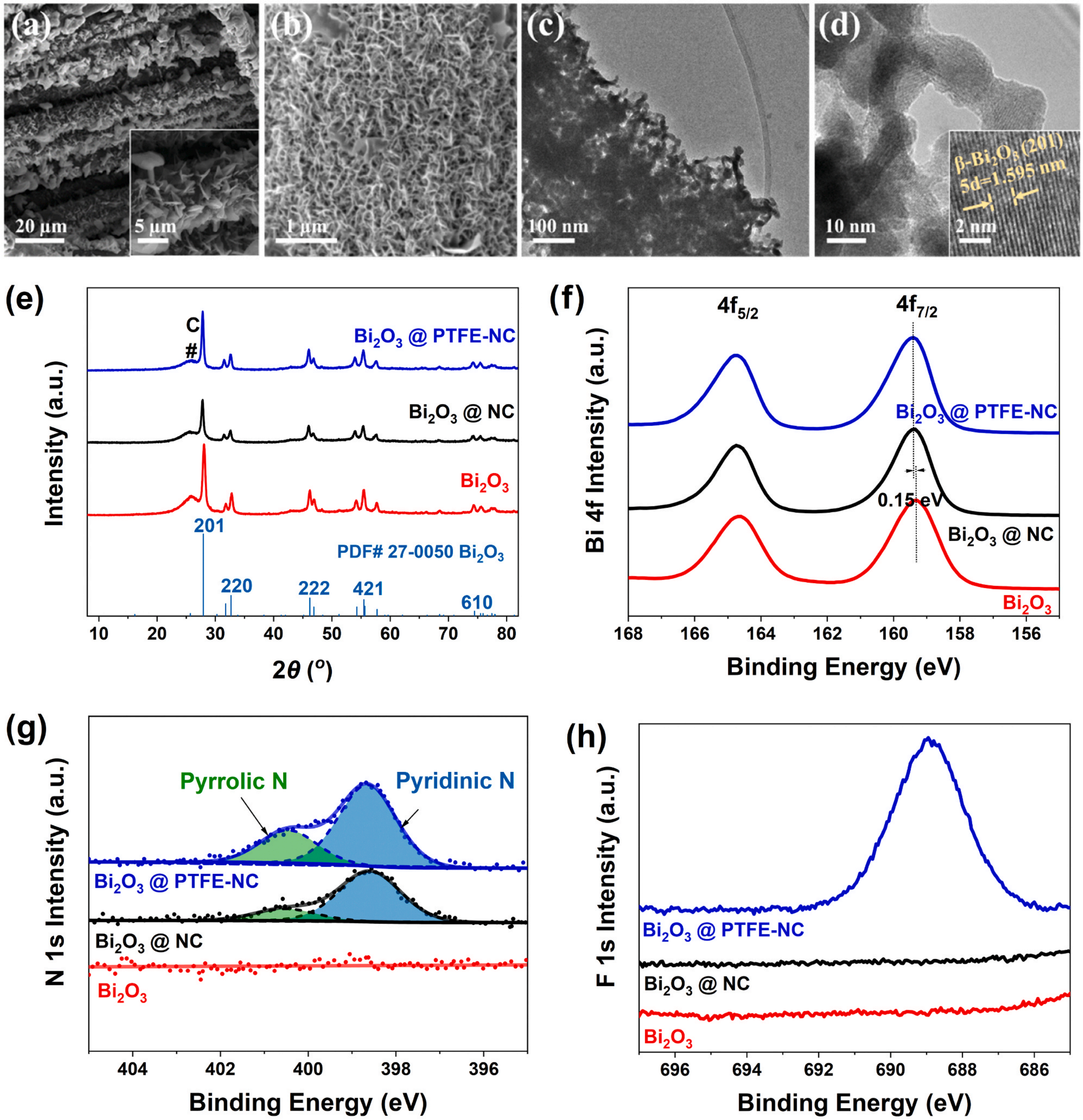

Fig. 1. Phys-chemical characterizations. SEM images of (a) the PTFE-NC support and (b) Bi_2O_3@PTFE-NC, (c) and (d) TEM images of Bi_2O_3 from Bi_2O_3@PTFE-NC. (e) XRD, (f) Bi 4 f high-resolution XPS spectra, (g) N 1 s high-resolution XPS spectra, and (h) F 1 s high-resolution XPS spectra of Bi_2O_3, Bi_2O_3@NC, and Bi_2O_3@PTFE-NC.

$$CO_2^{*-}(ads) + HCO_3^- \rightarrow HCOO^*(ads) + CO_3^{2-} \quad (3)$$

$$HCOO^*(ads) + e^- \rightarrow HCOO^-(ads) \quad (4)$$

$$HCOO^-(ads) \rightarrow HCOO^-(solution) \quad (5)$$

The enhancement in CO_2 sorption (Eq. (1)) and the enlarged ECSA offers an increasing number of active sites for the reaction. The lower charge transfer resistance in Bi_2O_3@NC compared to Bi_2O_3 indicates that CO_2 accepts more readily electrons to form CO_2^{*-} (Eq. (2)). Moreover, NC in the vicinity of Bi_2O_3 is reported to enhance adsorption capacity and lower the energy barrier to form formic acid intermediate ($HCOO^*$, Eq. (3)) [25,58]. To sum up, the performance boost after the introduction of NC near Bi_2O_3 could be attributed to multiple reasons as an enlarged ECSA, faster kinetics, enhanced charge transfer, and increase in the adsorption capacity of CO_2 and $HCOO^*$.

3.3. Modulations of surface hydrophobicity of the Bi_2O_3@NC electrode with tuning both support and catalyst layer with PTFE

However, when comparing the potential window where over 90% FE for formate is reached, a problem is evidently present on Bi_2O_3@NC. The FE for formate on Bi_2O_3@NC first drops to 86.3% at −1.17 V (vs. RHE) and further deteriorates to 73.3% at −1.37 V (vs. RHE), while Bi_2O_3 still retains a high value of 87.8% at −1.37 V (vs. RHE). The current density of competing H_2 production on Bi_2O_3@NC increases around 6 times at this potential when compared to Bi_2O_3 (Figure S6e). To understand what

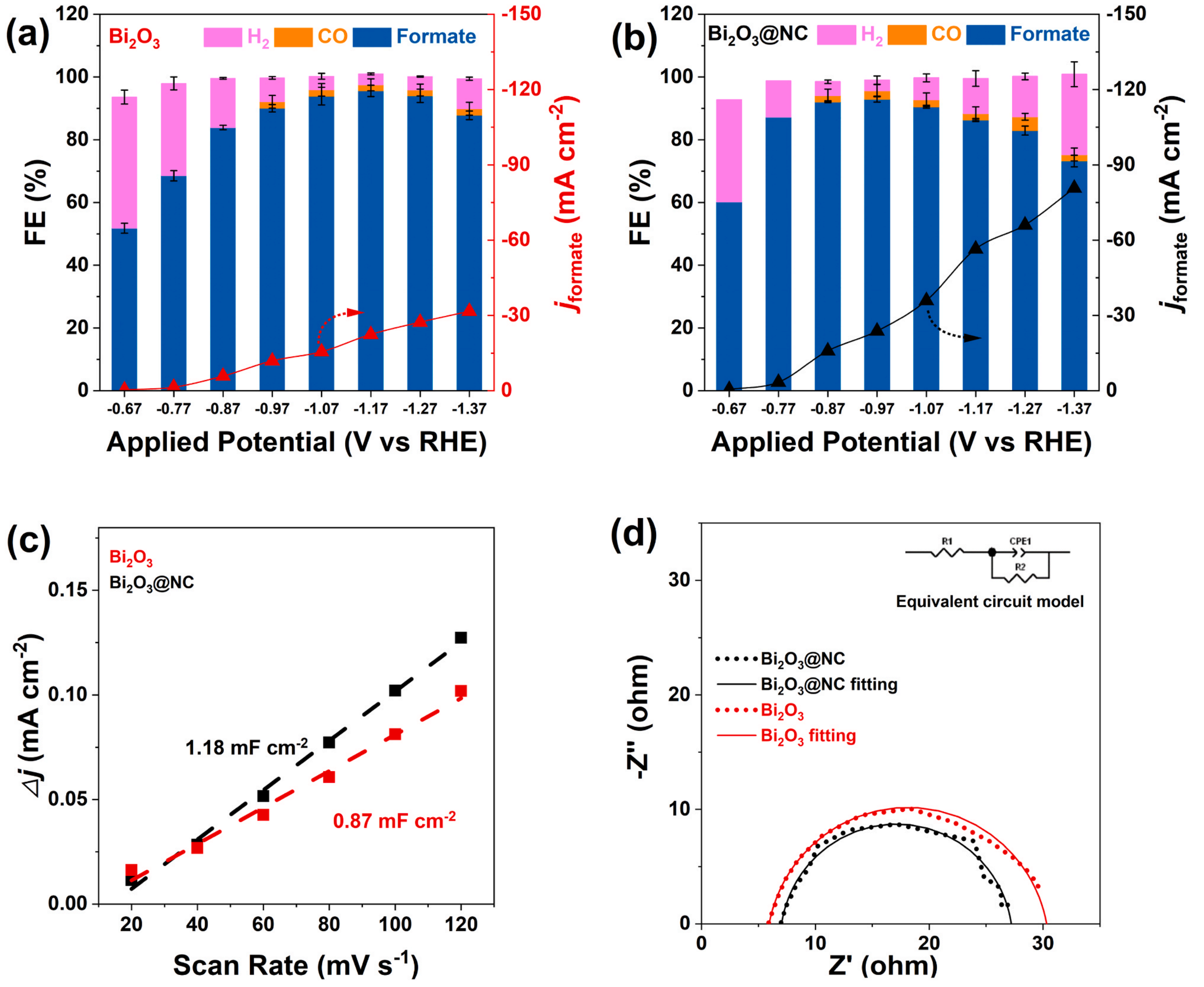

Fig. 2. Potential dependence of selectivity and partial *j* of formate over (a) Bi_2O_3 and (b) Bi_2O_3@NC. (c) Capacitive current plotted against the scan rate for Bi_2O_3 and Bi_2O_3@NC for the determination of C_{dl}. (d) Nyquist plots of Bi_2O_3 and Bi_2O_3@NC at −0.67 V (vs. RHE) with equivalent circuit model (R1: Ohmic resistance, R2: charge transfer resistance). All the measurements were conducted in CO_2-saturated 0.5 M $KHCO_3$ at room temperature.

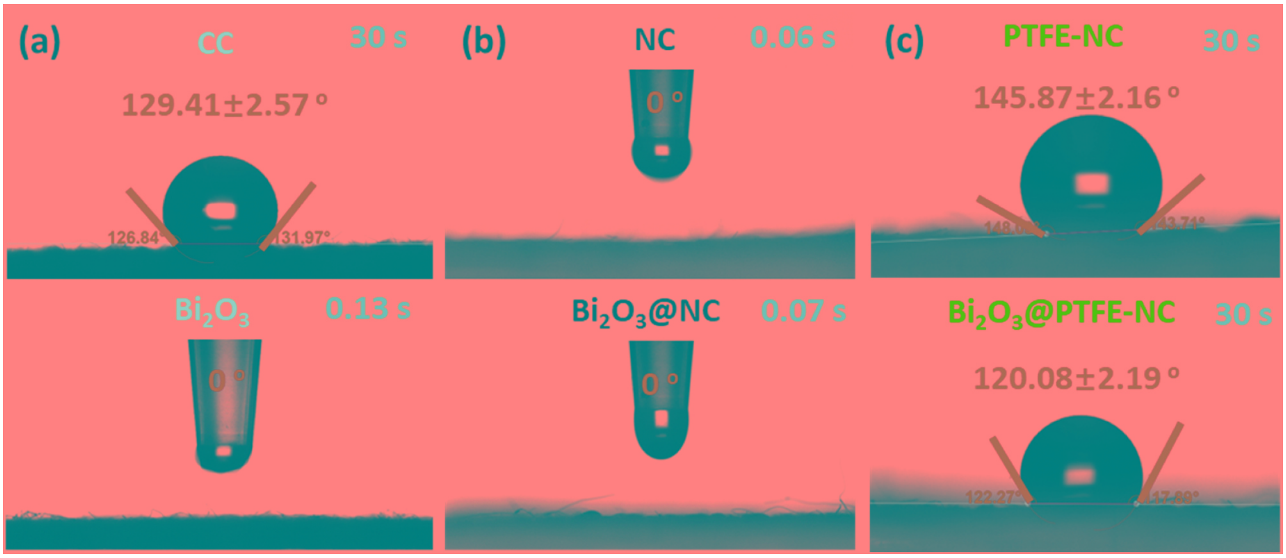

Fig. 3. Contact angle measurements of (a) CC and Bi_2O_3, (b) NC and Bi_2O_3@NC, and (c) PTFE-NC and Bi_2O_3@PTFE-NC (the image captured time is shown).

may cause this, we must look at the electrode structure more closely: It is generally recognized that CO_2RR occurs at the solid−liquid−gas triple-phase interface. Gaseous CO_2 transport is facilitated by the hydrophobic domains and the presence of these domains also prevents flooding from clogging the gas diffusion pathways. At the same time, protons and dissolved CO_2 molecules are transported with the electrolyte through the hydrated hydrophilic domains [59]. Bi_2O_3@NC exhibits a faster reaction rate of CO_2RR (higher partial current densities), and consequently enters the reactant diffusion-dominating potential region earlier than Bi_2O_3. Due to the low solubility of CO_2, the amount of dissolved CO_2 molecules delivered to the active sites through the electrolyte is insufficient for promoting the reaction in this region, which requires the diffusion of extra gaseous CO_2 towards active sites through hydrophobic domains [32,33]. The limiting current densities are reported to be inversely correlated with the length of the gaseous CO_2 diffusion pathway, especially at high overpotentials [60]. To decrease the length of those pathways, a better solid-liquid-gas triple-phase interface enhancing gaseous CO_2 transfer to the active site must be constructed.

According to the contact angle measurements presented in Fig. 3a, the surface of CC is hydrophobic while the porous Bi_2O_3 surface on CC shows a hydrophilic feature. In contrast, the electrolyte droplet is almost instantly absorbed by the surface as NC turns to be extremely hydrophilic (Fig. 3b). Growing hydrophilic Bi_2O_3 on the hydrophilic NC leads to an electrode (Bi_2O_3@NC) with super hydrophilicity (Fig. 3b). The loss of hydrophobic domains in Bi_2O_3@NC hinders gaseous CO_2 transport towards active Bi_2O_3 sites efficiently. Moreover, NC may also be activated and favor HER when in contact with protons [61]. When these two supports without Bi_2O_3 are directly utilized as the working electrode, NC exhibits partial current densities of HER that are around two times higher than those of bulk CC (Figure S9). Increasing proton consumption on NC also restricts the CO_2-to-formate since this conversion also includes a protonation process (Eq. (3)). As a result, selectivity to formate on Bi_2O_3@NC continues to decrease in the reactants (gaseous CO_2 and protons) diffusion-dominating potential region. There appears to be a trade-off between the improved adsorption of intermediates and the increased hydrophilicity brought by the introduction of NC which is evident also in previous studies [24].

To mitigate this issue, we adjusted the hydrophobicity of the electrode surface with a PTFE polymer. PTFE is a synthetic fluoropolymer, which is quite widely used in the electrochemistry field as a coating and binder because of its highly hydrophobic nature [35,41,62–65]. To obtain an ideal state, where sufficient hydrophobic regions to boost the transfer of reactants and sufficient hydrophilic regions to retain contact with the electrolyte exist [28], the PTFE content needs to be optimized. Electrodes were then fabricated to weigh the advantages and disadvantages of the two commonly used strategies, which are modulating either the hydrophobicity of the support surface or the catalyst surface using PTFE of different concentrations.

First, to modify the support surface (NC), PTFE solutions with varying concentrations were applied to treat NC using a dip coating method as described in Methods section. When PTFE modification is applied, HER is successfully inhibited to the same degree as on CC (Figure S9) and the surface becomes hydrophobic (Fig. 3c). After the PTFE modification, Bi_2O_3 was grown on these PTFE-modified NC supports (see **Methods** and Scheme 1). It is noteworthy that the hydrophilicity of the Bi_2O_3 surface has only a slight influence on the hydrophobicity of the entire electrode since Bi_2O_3@PTFE-NC is still hydrophobic (Fig. 3c), similar as earlier reported to Bi_2O_3 on hydrophobic carbon fiber [11]. To screen the ideal PTFE content, these samples were employed as the working electrodes for CO_2RR at −1.37 V (vs. RHE) (Fig. 4a). As the concentration of the PTFE solution used in the synthesis is increased to 0.2 wt%, the performance of CO_2RR is improved since the side reaction HER is suppressed while the total current density remains high (Fig. 4a). However, both FE of formate and total current density drop when the concentration of the PTFE solution is increased further from 0.2 wt%. This is probably due to that higher amount of insulating PTFE polymer particles cover the NC surfaces and disrupt the charge transfer.

The solid−liquid−gas triple-phase interface can also be enhanced by hydrophobicity modifications of the catalyst surface. The PTFE solutions with the same concentrations were applied to modify the Bi_2O_3@NC and these modified working electrodes were subsequently also evaluated at −1.37 V (vs. RHE) (Fig. 4b). We indeed notice a suppression of HER with the increasing PTFE coverage. However, this suppression comes at the expense of the total current density which continuously drops with more PTFE introduced. This is likely due to Bi_2O_3 surfaces being shielded by this insulating polymer (PTFE) from the catalytic reaction.

Both CO_2-to-formate and HER processes require proton transfer. With the wettability tuning of the support, there are fewer protons in contact with hydrophobic PTFE-NC to favor HER but enough protons are delivered to hydrophilic active sites for CO_2RR. Through this comparison, surface engineering of support surfaces by growing Bi_2O_3 on PTFE-NC is unquestionably a superior method over PTFE modification of the catalyst surface. Hence, for further experiments the concentration of the PTFE solution used to modify the NC supports was fixed to 0.2 wt% because it promotes the CO_2RR on the working electrode more than all other studied electrode modifications.

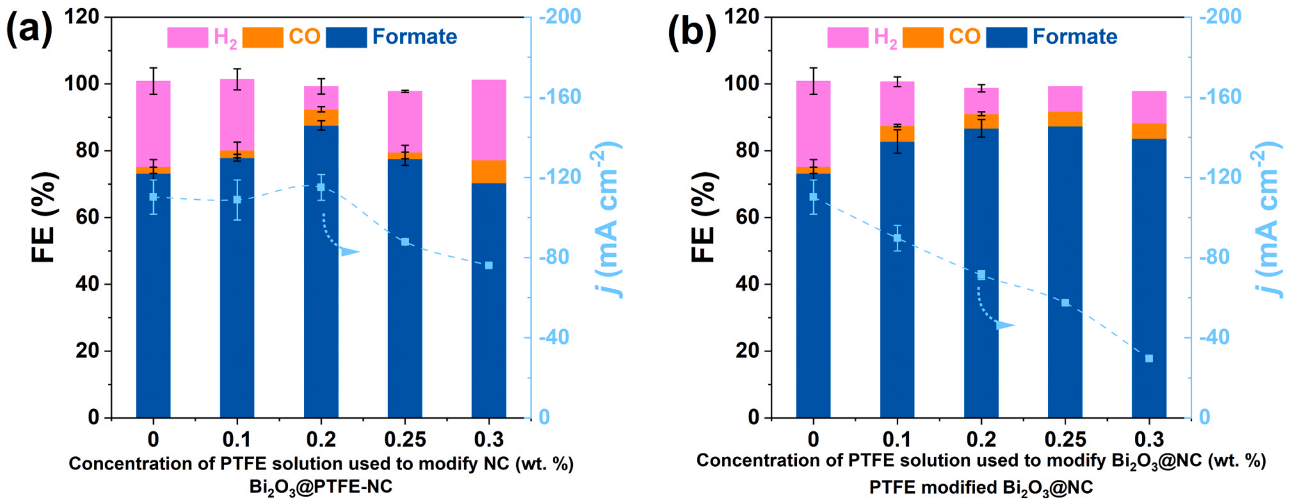

Fig. 4. Comparison of selectivity and total *j* at −1.37 V (vs. RHE) in CO_2-saturated 0.5 M $KHCO_3$ at room temperature between surface hydrophobicity tuning of (a) the support by modifying NC before Bi_2O_3 growth and (b) the catalyst layer by directly modifying Bi_2O_3@NC using PTFE of different concentrations.

3.4. Performance comparison of Bi_2O_3@PTFE-NC and Bi_2O_3@NC

Hydrophobicity of the electrodes is reported to evade the stability challenges due to flooding of the electrode [66]. To evaluate the stability of the differently modified electrodes, chronoamperometry at a fixed potential of −0.97 V (vs. RHE) was performed for several hours (Fig. 5a-b). The total current density and formate FE on Bi_2O_3@PTFE-NC does not noticeably decrease during the 12 h of electrolysis, indicating good stability of performance. Postmortem SEM analysis shows that the morphology is nanosheet (Figure S10a-b) while the XRD pattern (Figure S10c) shows a mixture of metallic Bi with some $Bi_2(CO_3)O_2$. This is in accordance with the reported literature [22,67]. The high-resolution XPS Bi spectrum in Figure S10d depicts that on the surface the chemical composition is Bi^{3+}, which may result from the re-oxidation of the metallic Bi or surface $Bi_2(CO_3)O_2$ as the sample has been under ambient conditions before the XPS measurements. The contact angle of the used electrode shows a slight decrease, but the electrode is still hydrophobic (Figure S11a), and the high-resolution F 1 s spectrum of XPS demonstrates that there is no chemical composition change of the PTFE during longer term electrolysis (Figure S11b).

In contrast, Bi_2O_3@NC only shows good selectivity towards formate production and inhibition of HER during the first 1 h of electrolysis. After that, flooding occurs since HER continues to rise so that FE towards formate declines gradually (Fig. 5b). The flooding worsens after 3 h and the total current density becomes quite unstable and starts to decrease, demonstrating that Bi_2O_3@NC is not suitable for long-term use. As shown previously, the electrolyte wets both NC and Bi_2O_3@NC immediately (Fig. 3b), which may block the gaseous CO_2 diffusion pathway to the active sites [66]. Consequently, it lowers CO_2 concentration at the catalyst/electrolyte interface causing CO_2RR to deteriorate. The electrolyte saturation can also promote salt precipitation, leading to the eventual permeant blockage of CO_2 diffusion and reduced active area [68].

To verify the stability improving effects of PTFE modified support, CC covered with PTFE was also used as a support for Bi_2O_3. Bi_2O_3@PTFE-CC exhibits similar short-term performance of CO_2-to-formate conversion in terms of FE and partial current density for formate production when compared with Bi_2O_3 (Figure S13a). However, Bi_2O_3@PTFE-CC shows stable behavior over 12 h of electrolysis while flooding occurs on Bi_2O_3 already after 2 h (Figure S13b-c) demonstrating that hydrophobicity modulation of supports is a universal method to improve the stability of CO_2RR.

To gain a more comprehensive electrochemical evaluation, short-term CO_2 electrolysis on the Bi_2O_3@PTFE-NC electrode was performed in a wider range of potentials and the results are compared with Bi_2O_3@NC (Figure S12 and Fig. 5c-d). Bi_2O_3@PTFE-NC shows similar onset potential and total current density to Bi_2O_3@ NC (Figure S12a-b), and the same three products —trace quantities of CO, primary formate, and the side product H_2 — are still detected in this potential range (Figure S12c). Compared to Bi_2O_3@NC, the formate FE on Bi_2O_3@PTFE-

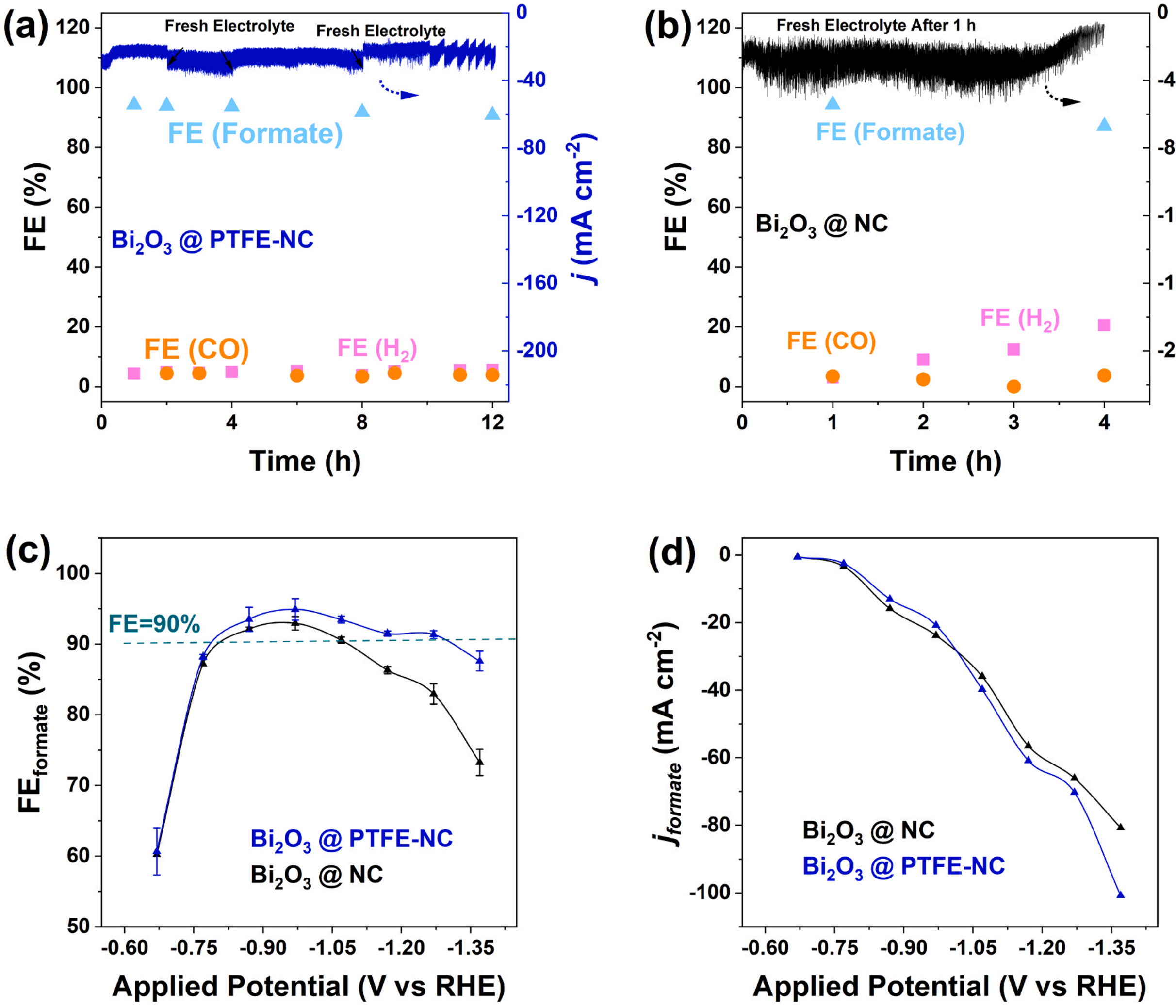

Fig. 5. Stability measurements at −0.97 V (vs. RHE) of (a) Bi_2O_3@PTFE-NC and (b) Bi_2O_3@NC. Potential dependence on (c) selectivity and (d) partial *j* of formate over Bi_2O_3@PTFE-NC and Bi_2O_3@NC. All the measurements were conducted in CO_2-saturated 0.5 M $KHCO_3$ at room temperature.

NC displays roughly the same values in the low overpotential region and only after applying more negative potentials the formate FE becomes noticeably higher (Fig. 5c and Table S1). For example, at an applied potential of −0.97 V (vs. RHE), the formate FE value reaches 94.9% on Bi_2O_3@PTFE-NC while it only reaches 92.9% for Bi_2O_3@NC at the same applied potential. Surprisingly, the FE for formate production is 87.6% at −1.37 V (vs. RHE) on Bi_2O_3@PTFE-NC, which is more than 14% higher than the value on Bi_2O_3@NC and approximately identical to the selectivity on Bi_2O_3 (87.8%) at the same applied potential. The PTFE modification broadens the potential range, where FE for formate production is ≥90%, to over 400 mV while the range is only 200 mV for Bi_2O_3@NC. When the partial current density towards formate production is plotted (Fig. 5d), Bi_2O_3@PTFE-NC exhibits a negligibly lower value at low overpotentials but a sound improvement starting from −1.07 V (vs. RHE) compared to Bi_2O_3@NC. Particularly at −1.37 V (vs. RHE), it has a 25% increase (−100.8 vs. −80.7 mA cm^{-2} for Bi_2O_3@PTFE-NC and Bi_2O_3@NC, respectively). A 60-hour electrolysis was performed at −0.87 V (vs. RHE), which is the potential of formate FE first reaches over 90% (Fig. 5c). The current density remains stable, and the formate FE undergoes only neglectable decay, still maintaining 87.6% even after 60 h (Figure S12d). The performance of CO_2RR, including the required overpotential, the partial current density, and the broad potential range for obtaining over 90% formate FE, is higher than many reported Bi-based working electrodes (see summarized CO_2RR performance of literature in Table S2).

This improvement in the formate FE at high overpotentials is not likely due to the charge transfer resistance and ECSA, since Bi_2O_3@PTFE-NC exhibits similar charge transfer resistance and lower ECSA compared to Bi_2O_3@NC (Figure S14). This improvement should originate from the enhanced gaseous CO_2 diffusion in this reactant diffusion-dominating potential region due to the hydrophobicity modulation. The hydrophobicity change can further restrict water diffusion and may generate a more alkaline microenvironment as reported [11,40]. In our flow-through cell configuration, CO_2 gas is directly bubbled onto and subsequently through the working electrode. Because of its hydrophobic feature in the air, we postulate that the Bi_2O_3@PTFE-NC has an aerophilic property in the water, whereas the hydrophilic Bi_2O_3@NC would be aerophobic. Both Bi_2O_3@PTFE-NC and Bi_2O_3@NC were subjected to a CO_2 bubble adhesion experiment in 0.5 M CO_2-saturated $KHCO_3$ solution and the results are presented in Fig. 6, and videos in **Appendix B-C**. The outcomes demonstrate that the CO_2 bubble can enter through the surface of Bi_2O_3@PTFE-NC extremely quickly (within 45 ms) confirming its aerophilic property (Fig. 6a and Video in **Appendix B**). It implies that the surface hydrophobicity of the electrode is a crucial factor in CO_2 gas transport. On the other hand, the CO_2 bubble is easily stuck on the surface of Bi_2O_3@NC (Fig. 6b and Video in **Appendix C**). Even in the flow-through flow cell, Bi_2O_3@NC probably could only utilize a relatively little amount of gaseous CO_2 for the reaction.

Hence, we suggest the coexistence of hydrophilic-hydrophobic domains in this electrode for maximum performance (Scheme 2a) where the hydrophobicity of the whole electrode surface is introduced by the super hydrophobic PTFE-NC support and the active sites are hydrophilic. Such a state can be called a Cassie-Wenzel coexistence state [32,42,69], where the surface is neither super hydrophilic nor superhydrophobic. In this state, not only the dissolved CO_2 is utilized in the reaction, but there can also be a concentrated CO_2 gas layer trapped near the aerophilic (hydrophobic) PTFE-NC support as earlier reported which can be used in the reaction [11,32]. In this scenario, the formation of the solid−liquid−gas triple-phase interface is boosted, making the active sites more accessible to both gaseous CO_2 and liquid electrolytes. Consequently, the CO_2 molecules from the gas phase, the ions (as proton source) from the liquid phase, and the electron transfer from the PTFE-NC support can greatly promote the CO_2RR at the triple-phase interface. Contrarily, the state of Bi_2O_3@NC is known as the Wenzel state because the active sites and the NC support are both super hydrophilic [32,42,69], and thus, the electrolyte can completely penetrate the electrode surface, preventing the creation of a triple-phase interface and almost eliminating the trapped CO_2 layer (Scheme 2b). In this case, only dissolved CO_2 molecules can get involved in the reaction which can hinder the reaction rate in the CO_2 diffusion-dominating potential region and leads to a drop in formate selectivity.

4. Conclusion

In conclusion, we fabricated a binder-free Bi_2O_3@NC electrode for CO_2RR. It exhibits enhanced performance at a low overpotential range compared with Bi_2O_3. Unfortunately, Bi_2O_3@NC suffers unfavorable side effects such as flooding during longer-term use and rapid drop in formate selectivity at a higher overpotential range. The problem is mitigated by tuning the hydrophobicity of the NC support with PTFE coverage before the Bi_2O_3 growth. The unique structure favors fast gaseous CO_2 transport without hindering the electrolyte contact with active sites of Bi_2O_3. The formation of hydrophilic (the Bi_2O_3 active sites) and hydrophobic (the PTFE-NC support) domains improved the solid−liquid−gas triple-phase interface enhancing gaseous CO_2 transfer to the active sites for CO_2RR. In addition, with the increasing surface hydrophobicity, the adverse contact between the electrolyte and support is reduced so that not only the competitive HER at high overpotentials is decreased but also flooding is inhibited. This work offers a facile way to fabricate binder-free electrodes and mitigate the flooding issue. It also

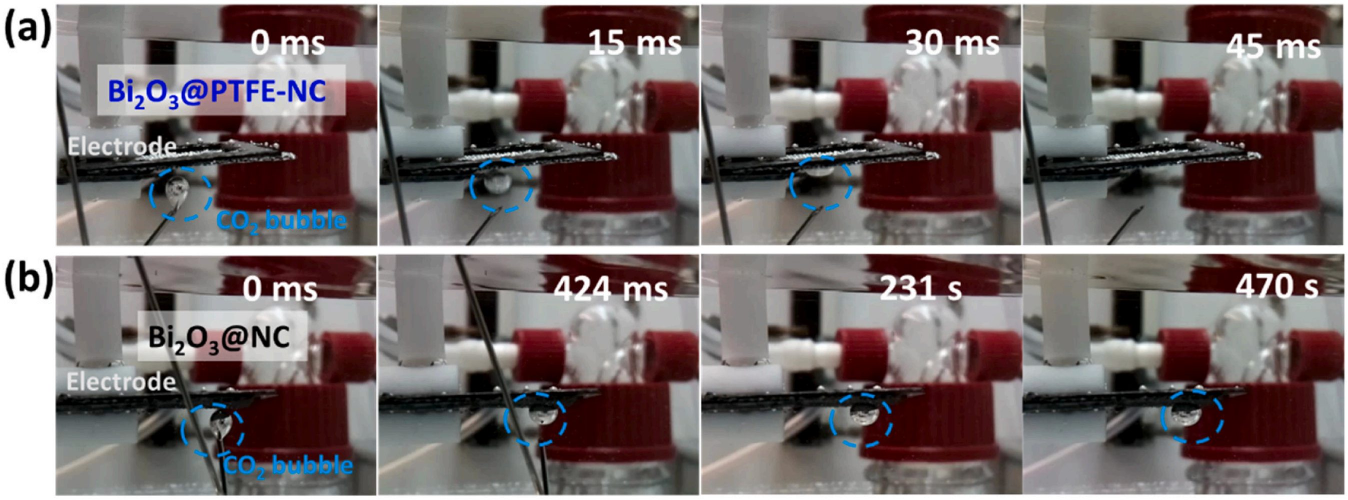

Fig. 6. CO_2 bubble adhesion experiment on (a) Bi_2O_3@PTFE-NC and (b) Bi_2O_3@NC.

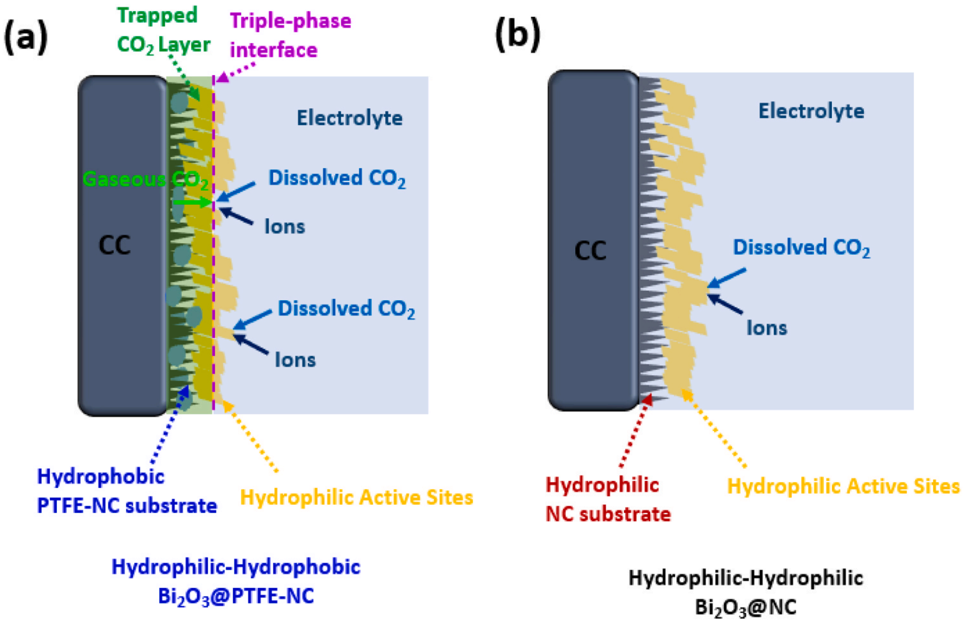

Scheme 2. Schematic illustration of (a) hydrophilic-hydrophobic domains in Bi_2O_3@PTFE-NC (both gaseous and dissolved CO_2 can be utilized in CO_2RR) and (b) hydrophilic-hydrophilic domains in Bi_2O_3@NC (only dissolved CO_2 can be utilized in CO_2RR).

rationally evaluates the benefits and drawbacks of the introduction of NC support of Bi-based electrocatalyst in CO_2RR. More importantly, the idea of construction of hydrophilic-hydrophobic domains in the electrode offers a possible way to alter the performance of other electrocatalytic reactions involving both gaseous/aqueous phases.

CRediT authorship contribution statement

Junjie Shi: Conceptualization, Methodology, Formal analysis, Investigation, Writing – original draft, Writing – review & editing. **Nana Han:** Methodology, Investigation, Formal analysis, Writing – review & editing. **Benjin Jin:** Investigation, Formal analysis, Writing – original draft, Writing – review & editing. **Milla Suominen:** Supervision, Investigation, Writing – review & editing, Data curation. **Jouko Lahtinen:** Investigation, Formal analysis, Writing – review & editing. **Kim Miikki:** Investigation, Writing – review & editing. **Benjamin P. Wilson:** Investigation, Writing – review & editing. **Tanja Kallio:** Conceptualization, Methodology, Supervision, Writing – review & editing, Resources, Data curation.

Declaration of Competing Interest

The authors declare that they have no known competing financial interests or personal relationships that could have appeared to influence the work reported in this paper

Acknowledgments

We acknowledge the provision of facilities and technical support by Aalto University at OtaNano - Nanomicroscopy Center (Aalto-NMC), BIOECONOMY, and RAMI infrastructures. We thank Jane and Aatos Erkko Foundation (the USVA project), the European Union's Horizon 2020 research and innovation programme under grant agreement HydrogenLung No. 892856, and Academy of Finland (the Profi 7 project, 142210501) for financial support. We thank Dr. Xiangze Kong for assistance in operating SEM-EDS.

Appendix A. Supporting information

Supplementary data associated with this article can be found in the online version at doi:10.1016/j.nxmate.2024.100183.

References

[1] D.U. Nielsen, X.M. Hu, K. Daasbjerg, T. Skrydstrup, Chemically and electrochemically catalysed conversion of CO_2 to CO with follow-up utilization to value-added chemicals, Nat. Catal. 1 (2018) 244–254, https://doi.org/10.1038/s41929-018-0051-3.

[2] Y. Pei, B. Zhang, Y. Lu, Carbon capture and utilization via electrochemistry, what's next, Nanotechnol 3–4 (2023) 100020, https://doi.org/10.1016/j.nxnano.2023.100020.

[3] N. Han, P. Ding, L. He, Y. Li, Y. Li, Promises of main group metal–based nanostructured materials for electrochemical CO_2 reduction to formate, Adv. Energy Mater. 10 (2020) 1–19, https://doi.org/10.1002/aenm.201902338.

[4] Y. Guan, M. Liu, X. Rao, Y. Liu, J. Zhang, Electrochemical reduction of carbon dioxide (CO_2): bismuth-based electrocatalysts, J. Mater. Chem. A 9 (2021) 13770–13803, https://doi.org/10.1039/d1ta01516h.

[5] D. Xia, H. Yu, H. Xie, P. Huang, R. Menzel, M.M. Titirici, G. Chai, Recent progress of Bi-based electrocatalysts for electrocatalytic CO_2 reduction, Nanoscale 14 (2022) 7957–7973, https://doi.org/10.1039/d2nr01900k.

[6] Z.B. Hoffman, T.S. Gray, Y. Xu, Q. Lin, T.B. Gunnoe, G. Zangari, High selectivity towards formate production by electrochemical reduction of carbon dioxide at copper–bismuth dendrites, ChemSusChem 12 (2019) 231–239, https://doi.org/10.1002/cssc.201801708.

[7] X. An, S. Li, X. Hao, X. Du, T. Yu, Z. Wang, X. Hao, A. Abudula, G. Guan, Thein situmorphology transformation of bismuth-based catalysts for the effective electroreduction of carbon dioxide, Sustain. Energy Fuels 4 (2020) 2831–2840, https://doi.org/10.1039/d0se00228c.

[8] J. Wang, J. Mao, X. Zheng, Y. Zhou, Q. Xu, Sulfur boosting CO_2 reduction activity of bismuth subcarbonate nanosheets via promoting proton-coupled electron transfer, Appl. Surf. Sci. 562 (2021) 150197, https://doi.org/10.1016/j.apsusc.2021.150197.

[9] M. Wu, Y. Xiong, B. Hu, Z. Zhang, B. Wei, L. Li, J. Hao, W. Shi, Indium doped bismuth subcarbonate nanosheets for efficient electrochemical reduction of carbon dioxide to formate in a wide potential window, J. Colloid Interface Sci. 624 (2022) 261–269, https://doi.org/10.1016/j.jcis.2022.05.054.

[10] S. Yang, M. Jiang, W. Zhang, Y. Hu, J. Liang, Y. Wang, Z. Tie, Z. Jin, In situ structure refactoring of bismuth nanoflowers for highly selective electrochemical reduction of CO_2 to formate, Adv. Funct. Mater. 33 (2023) 2301984, https://doi.org/10.1002/adfm.202301984.

[11] S.Q. Liu, E. Shahini, M.R. Gao, L. Gong, P.F. Sui, T. Tang, H. Zeng, J.L. Luo, Bi_2O_3 Nanosheets grown on carbon nanofiber with inherent hydrophobicity for high-performance CO_2 electroreduction in a wide potential window, ACS Nano 15 (2021) 17757–17768, https://doi.org/10.1021/acsnano.1c05737.

[12] P.F. Sui, M.R. Gao, S. Liu, C. Xu, M.N. Zhu, J.L. Luo, Carbon dioxide valorization via formate electrosynthesis in a wide potential window, Adv. Funct. Mater. 32 (2022) 2203794, https://doi.org/10.1002/adfm.202203794.

[13] L. Lin, X. He, X. Zhang, W. Ma, B. Zhang, D. Wei, S. Xie, Q. Zhang, X. Yi, Y. Wang, A nanocomposite of bismuth clusters and $Bi_2O_2CO_3$ sheets for highly efficient electrocatalytic reduction of CO_2 to formate, Angew. Chem. Int. Ed. 62 (2023) e202214959, https://doi.org/10.1002/anie.202214959.

[14] T. Gao, X. Wen, T. Xie, N. Han, K. Sun, L. Han, H. Wang, Y. Zhang, Y. Kuang, X. Sun, Morphology effects of bismuth catalysts on electroreduction of carbon dioxide into formate, Electrochim. Acta 305 (2019) 388–393, https://doi.org/10.1016/j.electacta.2019.03.066.

[15] M. Zhang, W. Wei, S. Zhou, D.D. Ma, A. Cao, X.T. Wu, Q.L. Zhu, Engineering a conductive network of atomically thin bismuthene with rich defects enables CO_2 reduction to formate with industry-compatible current densities and stability, Energy Environ. Sci. 14 (2021) 4998–5008, https://doi.org/10.1039/d1ee01495a.

[16] X. Li, X. Wu, J. Li, J. Huang, L. Ji, Z. Leng, N. Qian, D. Yang, H. Zhang, Sn-Doped Bi_2O_3 nanosheets for highly efficient electrochemical CO_2 reduction toward formate production, Nanoscale 13 (2021) 19610–19616, https://doi.org/10.1039/d1nr06038d.

[17] Y. Zhao, X. Liu, Z. Liu, X. Lin, J. Lan, Y. Zhang, Y.R. Lu, M. Peng, T.S. Chan, Y. Tan, Spontaneously Sn-doped Bi/BiO_x core-shell nanowires toward high-performance CO_2 electroreduction to liquid fuel, Nano Lett. 21 (2021) 6907–6913, https://doi.org/10.1021/acs.nanolett.1c02053.

[18] Z. Wang, Q. Yuan, J. Shan, Z. Jiang, P. Xu, Y. Hu, J. Zhou, L. Wu, Z. Niu, J. Sun, T. Cheng, W.A. Goddard, Highly selective electrocatalytic reduction of CO_2 into methane on Cu-Bi nanoalloys, J. Phys. Chem. Lett. 11 (2020) 7261–7266, https://doi.org/10.1021/acs.jpclett.0c01261.

[19] L. Li, A. Ozden, S. Guo, F.P. García de Arquer, C. Wang, M. Zhang, J. Zhang, H. Jiang, W. Wang, H. Dong, D. Sinton, E.H. Sargent, M. Zhong, Stable, active CO_2 reduction to formate via redox-modulated stabilization of active sites, Nat. Commun. 12 (2021) 1–9, https://doi.org/10.1038/s41467-021-25573-9.

[20] R. Yu, C. Qiu, Z. Lin, H. Liu, J. Gao, S. Li, Y. Yao, J. Yu, S. Yang, CeO_x promoted electrocatalytic CO_2 reduction to formate by assisting in the critical hydrogenation step, ACS Mater. Lett. 4 (2022) 1749–1755, https://doi.org/10.1021/acsmaterialslett.2c00512.

[21] J. Sun, W. Zheng, S. Lyu, F. He, B. Yang, Z. Li, L. Lei, Y. Hou, Bi/Bi_2O_3 nanoparticles supported on N-doped reduced graphene oxide for highly efficient CO_2 electroreduction to formate, Chin. Chem. Lett. 31 (2020) 1415–1421, https://doi.org/10.1016/j.cclet.2020.04.031.

[22] S. Liu, X.F. Lu, J. Xiao, X. Wang, X.W. (David Lou, Bi_2O_3 nanosheets grown on multi-channel carbon matrix to catalyze efficient CO_2 electroreduction to HCOOH, Angew. Chem. Int. Ed. 58 (2019) 13828–13833, https://doi.org/10.1002/anie.201907674.

[23] X. Wang, W.-J. Yin, Y. Si, X. Wang, X. Guo, W. Guo, Y. Fu, Conversion of CO_2 to chemical feedstocks over bismuth nanosheets in situ grown on nitrogen-doped carbon, J. Mater. Chem. A 8 (2020) 19938–19945, https://doi.org/10.1039/D0TA07411J.

[24] F. Meng, Q. Zhang, K. Liu, X. Zhang, Integrated bismuth oxide ultrathin nanosheets/carbon foam electrode for highly selective and energy-efficient electrocatalytic conversion of CO_2 to HCOOH, Chem. Eur. J. 26 (2020) 4013–4018, https://doi.org/10.1002/chem.201903158.

[25] Z. Chen, D. Zhang, H. Zhang, H. Li, J. Zhou, L. Liu, X. He, Nitrogen-doped carbon nanofibers confined bismuth oxide nanocrystals boost high single-pass CO_2-to-formate conversion in large area membrane electrode assembly electrolyzers, Appl. Surf. Sci. 620 (2023) 156867, https://doi.org/10.1016/j.apsusc.2023.156867.

[26] D. Wu, G. Huo, W.Y. Chen, X.Z. Fu, J.L. Luo, Boosting formate production at high current density from CO_2 electroreduction on defect-rich hierarchical mesoporous Bi/Bi_2O_3 junction nanosheets, Appl. Catal. B 271 (2020) 118957, https://doi.org/10.1016/j.apcatb.2020.118957.

[27] H. Sun, J. Zhu, D. Baumann, L. Peng, Y. Xu, I. Shakir, Y. Huang, X. Duan, Hierarchical 3D electrodes for electrochemical energy storage, Nat. Rev. Mater. 4 (2019) 45–60, https://doi.org/10.1038/s41578-018-0069-9.

[28] H. Yang, Q. Lin, Y. Wu, G. Li, Q. Hu, X. Chai, X. Ren, Q. Zhang, J. Liu, C. He, Highly efficient utilization of single atoms via constructing 3D and free-standing electrodes for CO_2 reduction with ultrahigh current density, Nano Energy 70 (2020) 104454, https://doi.org/10.1016/j.nanoen.2020.104454.

[29] Z. Chen, G. Yu, B. Li, X. Zhang, M. Jiao, N. Wang, X. Zhang, L. Liu, In situ carbon encapsulation confined nickel-doped indium oxide nanocrystals for boosting CO_2 electroreduction to the industrial level, ACS Catal. 11 (2021) 14596–14604, https://doi.org/10.1021/acscatal.1c04182.

[30] R. Chen, H.Y. Su, D. Liu, R. Huang, X. Meng, X. Cui, Z.Q. Tian, D.H. Zhang, D. Deng, Highly selective production of ethylene by the electroreduction of carbon monoxide, Angew. Chem. Int. Ed. 59 (2020) 154–160, https://doi.org/10.1002/anie.201910662.

[31] B.A.W. Mowbray, D.J. Dvorak, N. Taherimakhsousi, C.P. Berlinguette, How Catalyst dispersion solvents affect CO_2 electrolyzer gas diffusion electrodes, Energy Fuels 35 (2021) 19178–19184, https://doi.org/10.1021/acs.energyfuels.1c01731.

[32] R. Shi, J. Guo, X. Zhang, G.I.N. Waterhouse, Z. Han, Y. Zhao, L. Shang, C. Zhou, L. Jiang, T. Zhang, Efficient wettability-controlled electroreduction of CO_2 to CO at Au/C interfaces, Nat. Commun. 11 (2020) 1–10, https://doi.org/10.1038/s41467-020-16847-9.

[33] H. Jiang, R. Luo, Y. Li, W. Chen, Recent advances in solid–liquid–gas three-phase interfaces in electrocatalysis for energy conversion and storage, EcoMat 4 (2022) e1219, https://doi.org/10.1002/eom2.12199.

[34] X. Yang, Q. Li, S. Chi, H. Li, Y. Huang, R. Cao, Hydrophobic perfluoroalkane modified metal-organic frameworks for the enhanced electrocatalytic reduction of CO_2, SmartMat 3 (2022) 163–172, https://doi.org/10.1002/smm2.1086.

[35] R. Chen, W. Tian, Y. Jia, W. Xu, F. Chen, X. Duan, Q. Xie, C. Hu, W. Liu, Y. Zhao, Y. Kuang, Y. Zhang, X. Sun, Engineering interfacial aerophilicity of nickel-embedded nitrogen-doped CNTs for electrochemical CO_2 reduction, ACS Appl. Energy Mater. 2 (2019) 3991–3998, https://doi.org/10.1021/acsaem.9b00395.

[36] K.G. Schmitt, A.A. Gewirth, In situ surface-enhanced raman spectroscopy of the electrochemical reduction of carbon dioxide on silver with 3,5-diamino-1,2,4-triazole, J. Phys. Chem. C. 118 (2014) 17567–17576, https://doi.org/10.1021/jp503598y.

[37] D. Wakerley, S. Lamaison, F. Ozanam, N. Menguy, D. Mercier, P. Marcus, M. Fontecave, V. Mougel, Bio-inspired hydrophobicity promotes CO_2 reduction on a Cu surface, Nat. Mater. 18 (2019) 1222–1227, https://doi.org/10.1038/s41563-019-0445-x.

[38] G. Ma, O.A. Syzgantseva, Y. Huang, D. Stoian, J. Zhang, S. Yang, W. Luo, M. Jiang, S. Li, C. Chen, M.A. Syzgantseva, S. Yan, N. Chen, L. Peng, J. Li, B. Han, A hydrophobic Cu/Cu_2O sheet catalyst for selective electroreduction of CO to ethanol, Nat. Commun. 14 (2023) 1–9, https://doi.org/10.1038/s41467-023-36261-1.

[39] Z.Z. Niu, F.Y. Gao, X.L. Zhang, P.P. Yang, R. Liu, L.P. Chi, Z.Z. Wu, S. Qin, X. Yu, M. R. Gao, Hierarchical copper with inherent hydrophobicity mitigates electrode flooding for high-rate CO_2 electroreduction to multicarbon products, J. Am. Chem. Soc. 143 (2021) 8011–8021, https://doi.org/10.1021/jacs.1c01190.

[40] H.Q. Liang, S. Zhao, X.M. Hu, M. Ceccato, T. Skrydstrup, K. Daasbjerg, Hydrophobic copper interfaces boost electroreduction of carbon dioxide to ethylene in water, ACS Catal. 11 (2021) 958–966, https://doi.org/10.1021/acscatal.0c03766.

[41] L.S. Zhan, Y.C. Wang, M.J. Liu, X. Zhao, J. Wu, X. Xiong, Y.P. Lei, Hydropathy modulation on Bi_2S_3 for enhanced electrocatalytic CO_2 reduction, Rare Met. 42 (2022) 806–812, https://doi.org/10.1007/s12598-022-02212-w.

[42] H. Rabiee, L. Ge, J. Zhao, X. Zhang, M. Li, S. Hu, S. Smart, T.E. Rufford, Z. Zhu, H. Wang, Z. Yuan, Regulating the reaction zone of electrochemical CO_2 reduction on gas-diffusion electrodes by distinctive hydrophilic-hydrophobic catalyst layers, Appl. Catal. B 310 (2022) 121362, https://doi.org/10.1016/j.apcatb.2022.121362.

[43] L. Xiong, X. Fu, Y. Zhou, P. Nian, Z. Wang, Q. Yue, Precise site-hydrophobicity modulation for boosting high-performance CO_2 electroreduction, ACS Catal. 13 (2023) 6652–6660, https://doi.org/10.1021/acscatal.2c06106.

[44] W. Xie, H. Li, G. Cui, J. Li, Y. Song, S. Li, X. Zhang, J.Y. Lee, M. Shao, M. Wei, NiSn atomic pair on an integrated electrode for synergistic electrocatalytic CO_2 reduction, Angew. Chem. Int. Ed. 60 (2021) 7382–7388, https://doi.org/10.1002/anie.202014655.

[45] M. Chen, J. Bi, X. Huang, T. Wang, Z. Wang, H. Hao, Bi_2O_3 nanosheets arrays in-situ decorated on carbon cloth for efficient electrochemical reduction of nitrate, Chemosphere 278 (2021) 130386, https://doi.org/10.1016/j.chemosphere.2021.130386.

[46] L. Zhang, Y. Shi, Z. Wang, C. Hu, B. Shi, X. Cao, Porous β-Bi_2O_3 with multiple vacancy associates on highly exposed active {220} facets for enhanced photocatalytic activity, Appl. Catal. B 265 (2020) 118563, https://doi.org/10.1016/j.apcatb.2019.118563.

[47] L. Lin, H. Li, Y. Wang, H. Li, P. Wei, B. Nan, R. Si, G. Wang, X. Bao, Temperature-dependent CO_2 electroreduction over Fe-N-C and Ni-N-C single-atom catalysts, Angew. Chem. Int. Ed. 60 (2021) 26582–26586, https://doi.org/10.1002/anie.202113135.

[48] K. Miikki, A. Karakoç, M. Rafiee, D.W. Lee, J. Vapaavuori, J. Tersteegen, L. Lemetti, J. Paltakari, An open-source camera system for experimental measurements, SoftwareX 14 (2021) 100688, https://doi.org/10.1016/j.softx.2021.100688.

[49] M.N. Hossain, R. Khakpour, M. Busch, M. Suominen, K. Laasonen, T. Kallio, Temperature-controlled syngas production via electrochemical CO_2 reduction on a CoTPP/MWCNT composite in a flow cell, ACS Appl. Energy Mater. 6 (2023) 267–277, https://doi.org/10.1021/acsaem.2c02873.

[50] M. Ayiania, E. Weiss-Hortala, M. Smith, J.S. McEwen, M. Garcia-Perez, Microstructural analysis of nitrogen-doped char by Raman spectroscopy: Raman shift analysis from first principles, Carbon 167 (2020) 559–574, https://doi.org/10.1016/j.carbon.2020.05.055.

[51] H. Yang, M. Driess, P.W. Menezes, Self-supported electrocatalysts for practical water electrolysis, Adv. Energy Mater. 11 (2021) 2102074, https://doi.org/10.1002/aenm.202102074.

[52] C. Yu, P. Yang, L. Tie, S. Yang, S. Dong, J. Sun, J. Sun, One-pot fabrication of β-Bi_2O_3@Bi_2S_3 hierarchical hollow spheres with advanced sunlight photocatalytic RhB oxidation and Cr(VI) reduction activities, Appl. Surf. Sci. 455 (2018) 8–17, https://doi.org/10.1016/j.apsusc.2018.04.201.

[53] Y. Shi, L. Luo, Y. Zhang, Y. Chen, S. Wang, L. Li, Y. Long, F. Jiang, Synthesis and characterization of α/β-Bi_2O_3 with enhanced photocatalytic activity for 17α-ethynylestradiol, Ceram. Int. 43 (2017) 7627–7635, https://doi.org/10.1016/j.ceramint.2017.03.057.

[54] J. In, I. Yoon, K. Seo, J. Park, J. Choo, Y. Lee, B. Kim, Polymorph-tuned synthesis of α- and β-Bi_2O_3 nanowires and determination of their growth direction from polarized raman single nanowire microscopy, Chem. Eur. J. 17 (2011) 1304–1309, https://doi.org/10.1002/chem.201001684.

[55] X. Ma, L. Li, R. Chen, C. Wang, H. Li, H. Li, Highly nitrogen-doped porous carbon derived from zeolitic imidazolate framework-8 for CO_2 capture, Chem. Asian J. 13 (2018) 2069–2076, https://doi.org/10.1002/asia.201800548.

[56] N. Han, Y. Wang, H. Yang, J. Deng, J. Wu, Y. Li, Y. Li, Ultrathin bismuth nanosheets from in situ topotactic transformation for selective electrocatalytic CO_2 reduction to formate, Nat. Commun. 9 (2018) 1–8, https://doi.org/10.1038/s41467-018-03712-z.

[57] P. Deng, H. Wang, R. Qi, J. Zhu, S. Chen, F. Yang, L. Zhou, K. Qi, H. Liu, B.Y. Xia, Bismuth oxides with enhanced bismuth-oxygen structure for efficient electrochemical reduction of carbon dioxide to formate, ACS Catal. 10 (2020) 743–750, https://doi.org/10.1021/acscatal.9b04043.

[58] Z. Chen, K. Mou, X. Wang, L. Liu, Nitrogen-doped graphene quantum dots enhance the activity of Bi_2O_3 nanosheets for electrochemical reduction of CO_2 in a wide

negative potential region, Angew. Chem. Int. Ed. 57 (2018) 12790–12794, https://doi.org/10.1002/anie.201807643.

[59] H. Rabiee, L. Ge, X. Zhang, S. Hu, M. Li, Z. Yuan, Gas diffusion electrodes (GDEs) for electrochemical reduction of carbon dioxide, carbon monoxide, and dinitrogen to value-added products: a review, Energy Environ. Sci. 14 (2021) 1959–2008, https://doi.org/10.1039/d0ee03756g.

[60] Y. Chen, N.S. Lewis, C. Xiang, Modeling the performance of a flow-through gas diffusion electrode for electrochemical reduction of CO or CO_2, J. Electrochem. Soc. 167 (2020) 114503, https://doi.org/10.1149/1945-7111/ab987a.

[61] G. fa Long, K. Wan, M. yao Liu, Z. xing Liang, J. hua Piao, P. Tsiakaras, Active sites and mechanism on nitrogen-doped carbon catalyst for hydrogen evolution reaction, J. Catal. 348 (2017) 151–159, https://doi.org/10.1016/j.jcat.2017.02.021.

[62] Q. Wang, H. Dong, H. Yu, H. Yu, Enhanced performance of gas diffusion electrode for electrochemical reduction of carbon dioxide to formate by adding polytetrafluoroethylene into catalyst layer, J. Power Sources 279 (2015) 1–5, https://doi.org/10.1016/j.jpowsour.2014.12.118.

[63] Z. Jiang, Z. Zhang, H. Li, Y. Tang, Y. Yuan, J. Zao, H. Zheng, Y. Liang, Molecular catalyst with near 100% selectivity for CO_2 reduction in acidic electrolytes, Adv. Energy Mater. 13 (2023) 2–9, https://doi.org/10.1002/aenm.202203603.

[64] L. Li, J. Chen, V.S.S. Mosali, Y. Liang, A.M. Bond, Q. Gu, J. Zhang, Hydrophobicity graded gas diffusion layer for stable electrochemical reduction of CO_2, Angew. Chem. Int. Ed. 61 (2022) e202208534, https://doi.org/10.1002/anie.202208534.

[65] X. Sheng, W. Ge, H. Jiang, C. Li, Engineering the Ni-N-C catalyst microenvironment enabling CO_2 electroreduction with nearly 100% CO selectivity in acid, Adv. Mater. 34 (2022) 1–8, https://doi.org/10.1002/adma.202201295.

[66] K. Yang, R. Kas, W.A. Smith, T. Burdyny, Role of the carbon-based gas diffusion layer on flooding in a gas diffusion electrode cell for electrochemical CO_2 reduction, ACS Energy Lett. 6 (2021) 33–40, https://doi.org/10.1021/acsenergylett.0c02184.

[67] A. Dutta, I. Zelocualtecatl Montiel, K. Kiran, A. Rieder, V. Grozovski, L. Gut, P. Broekmann, A tandem ($Bi_2O_3 \rightarrow Bi_{met}$) catalyst for highly efficient *ec*-CO_2 conversion into formate: *Operando* Raman spectroscopic evidence for a reaction pathway change, ACS Catal. 11 (2021) 4988–5003, https://doi.org/10.1021/acscatal.0c05317.

[68] M.R. Singh, E.L. Clark, A.T. Bell, Effects of electrolyte, catalyst, and membrane composition and operating conditions on the performance of solar-driven electrochemical reduction of carbon dioxide, Phys. Chem. Chem. Phys. 17 (2015) 18924–18936, https://doi.org/10.1039/c5cp03283k.

[69] M. Li, M.N. Idros, Y. Wu, T. Burdyny, S. Garg, X.S. Zhao, G. Wang, T.E. Rufford, The role of electrode wettability in electrochemical reduction of carbon dioxide, J. Mater. Chem. A 9 (2021) 19369–19409, https://doi.org/10.1039/d1ta03636j.